Materials Science in Semiconductor Processing 186 (2025) 109073

Contents lists available at ScienceDirect

Materials Science in Semiconductor Processing

journal homepage: www.elsevier.com/locate/mssp

Tuning of electrical properties and persistent photoconductivity of SnO_2 thin films via La doping for optical memory applications

P. Asha Hind [a], Pawan Kumar [b], U.K. Goutam [c], B.V. Rajendra [a,*]

[a] Department of Physics, Manipal Institute of Technology, Manipal Academy of Higher Education, Manipal, 576104, India
[b] Department of Physics, Acharya Institute of Technology, Bangalore, 560107, India
[c] Technical Physics Division, Bhabha Atomic Research Centre, Mumbai, 400085, India

ARTICLE INFO

Keywords:
Tin oxide
Lanthanum doping
Spray pyrolysis
Persistent photoconductivity
Artificial synapse application

ABSTRACT

This work explored the potential of utilizing Lanthanum doped tin oxide $Sn_{1-x}La_xO_2$ (x = 0.01 to 0.1) based Metal-Semiconductor-Metal Ohmic photoconductors for optical memory applications making use of the persistent photoconductivity (PPC) property. The structural, optical, and electrical properties of $Sn_{1-x}La_xO_2$ thin films deposited on glass substrates using the spray pyrolysis method, with a focus on the impact of lanthanum concentration on the photoresponse characteristics was investigated. Raman spectroscopy confirmed the presence of oxygen vacancies and nanometric grain size in the films along with the typical Raman active modes of tin oxide. The Sn^{4+} and La^{3+} oxidation states in $Sn_{1-x}La_xO_2$ as well as the contributions from lattice oxygen and oxygen vacancies were identified using XPS. Photoluminescence studies revealed emissions in the UV, violet, blue, and yellow regions, corresponding to tin interstitials, oxygen vacancies, and other defects, with intensity variations based on La concentration. All films exhibited n-type conductivity, with La content influencing both resistivity and carrier concentration. Photoconductivity measurements demonstrated enhanced photocurrent under UV illumination, with La doping affecting energy levels and defect states. The $Sn_{0.90}La_{0.10}O_2$ film possessed a photocurrent retention of nearly 64 % within a span of 10^4 s, showing that higher concentration of La favoured the enhancement of retention of photocurrent for a comparatively longer duration. The significant persistent photoconductivity requires the conditions like optically active materials, a built-in electric field to separate electron-hole pairs, and defect states to trap carriers, which are all met by the prepared $Sn_{1-x}La_xO_2$ photoconductor with higher La doping levels, confirming the suitability of these films for practical use as optical non-volatile memory elements.

1. Introduction

Recent studies have revealed that oxide semiconductors can perform non-volatile storage tasks by harnessing the persistent photocurrent (PPC) properties. These materials retain their conductivity patterns even after the light source is removed, mimicking the retention of memory or information storage. This property allows for the creation of connections that can be programmed and adjusted based on light exposure. The persistent photoconductivity effect of oxide semiconductors aids in attaining slower decay and modulation of charge carriers effectively conducive to long-term memory [1]. In the pursuit of finding an efficient candidate for bringing this PPC effect to technology, metal oxides like tin oxide are very suitable choices by virtue of their defect structure. Tin oxide (SnO_2), commonly known as stannic oxide, is an important material with a variety of applications due to its interesting electronic and optical properties. It is a wide bandgap semiconductor with a band gap of about 3.6 eV and rutile-type tetragonal structure [2]. It usually exhibits n-type conductivity and transparency in the visible spectral region. Due to its transparency and electrical conductivity, it is used in applications such as transparent electrodes in displays, solar cells, photocatalytic applications, lithium-ion batteries and supercapacitors. It exhibits PPC due to its unique electronic and defect properties. The concentration and type of defects, such as oxygen vacancies and tin interstitials, significantly influence the degree of PPC. The PPC in SnO_2 can be exploited for non-volatile memory devices, where data can be stored in the form of persistent conductivity states [3]. Different strategies are employed for this, including extrinsic doping. The integration of rare earth (RE) dopants further enhances these properties. The RE

* Corresponding author.
E-mail address: bv.rajendra@manipal.edu (B.V. Rajendra).

https://doi.org/10.1016/j.mssp.2024.109073
Received 5 September 2024; Received in revised form 21 October 2024; Accepted 31 October 2024
Available online 2 November 2024

element Lanthanum (La) doping into SnO_2 lattice can influence the electrical conductivity, or it may introduce additional charge carriers or modify the band structure of the host. Moreover, Lanthanum oxide (La_2O_3) is also used for non-volatile memories as they are expected to crystallize above 400 °C in the hexagonal phase [4]. Thus, the inherent photoconductivity of the metal oxide semiconductor, coupled with the controllable doping of rare earth elements, can be analysed for their effectiveness in optically programmable memories.

Despite being a versatile material with assured tunability via doping, only a very few reports are available on doped SnO_2 thin films discussing different aspects of photosensing behaviour. In literature, Viana et al. [5] studied the PPC effect in individual nanobelts of SnO_2 as a function of temperature, in different atmospheres like air, helium, and vacuum, and low temperature. It was observed that under UV exposure and at temperatures of 200–400 K, there was enhanced photoconductivity, and the photocurrent increased as either the temperature or oxygen concentration decreased. Tierney et al. [6] reported that PPC had been observed in SnO_2 thin films prepared using RF sputtering upon illumination with a range of peak energies below band gap. They suggested that more than one mechanism accounted for PPC by noting the response patterns and the photocurrent decay as a function of photon energy under vacuum and at atmospheric pressure at room temperature as well. A model for photoconductivity at room temperature in nanocrystalline SnO_2 under illumination at energy below the fundamental band gap of SnO_2 was proposed by Brinzari [7]. The study focussed on electronic states situated at the bottom part of the band gap. These states were found to be related to oxygen vacancies at surface and Sn-derived electronic states. The study analysed the photoconductivity response and decay using numerical simulation based on balance rate equations for excited electrons and immobile holes. A correlation between the optoelectronic and transport properties of SnO_2 nanowires and their intrinsic defects pertaining to metastable state was investigated by Costa et al. [8]. The metastable defect associated with the green-emitting centre was found to be responsible for the anomalous behaviour observed in the temperature-dependent resistivity curves of ohmic single-nanowire devices when exposed to light. The photoconductivity measurements revealed two activation energies for a single nanowire, one with a value of 7 meV for temperatures below 100 K, consistent with the small value obtained in the photoluminescence experiments for the green-emitting centre, and the other with a higher activation energy of 220 meV for temperatures above 100 K. However, the application part of PPC phenomenon stays rather unexplored in the case of SnO_2 yet. To list a few similar works with other materials, Sun et al. [9] demonstrated a reconfigurable optical memory based on a MoS_2/quantum dots (QDs) heterostructure, exploiting the unique photoelectric coupling effect between MoS_2 and QDs to induce continuous n-doping and generate PPC. Similarly, Dai et al. [10] achieved giant photo-to-dark current ratios and long-lasting PPC in phototransistors using amorphous indium−gallium−zinc oxide and graphene nanosheets nanocomposites. Gadelha et al. [11] illustrated the possibility of non-volatile photo--memory in MoS_2 transistors, with high on/off ratios and long memory retention, achieved via laser-induced doping and PPC. Abbas et al. [12] demonstrated a transparent and flexible In_2O_3 thin film photo-memory with high persistence, suitable for multilevel data storage. Dixit et al. [13] observed long-lasting PPC in Au-coated CuO thin films, proposing optical excitation for set and reset processes. Lee et al. [14] reported giant PPC in VO_2 film devices for potential applications in optical remote control of electronic devices like optical memories. These studies showcase the versatility and potential of PPC across a range of materials and device architectures for optical memory applications.

Thus, the objective of this study is to explore the influence of lanthanum concentration on the structural, optical, and electrical properties of $Sn_{1-x}La_xO_2$ (x = 0.01 to 0.1) films deposited on glass substrates using the spray pyrolysis method. By investigating the role of La doping on oxygen vacancies, grain size, and defect levels, the research aims to understand how varying La content affects the photoconductivity, resistivity, and carrier concentration of the films. Special attention is given to the impact of La on the photocurrent decay behaviour, with the goal of identifying the potential of these films for use in optical memory devices due to their persistent photocurrent response. Moreover, the utilization of rare earth doped tin oxide thin films as the active material in Metal-Semiconductor-Metal (MSM) Ohmic photoconductors is also explored.

2. Materials and methods

The $Sn_{1-x}La_xO_2$ (x = 0.01 to 0.1) thin films were deposited on chemically cleaned glass substrates using spray pyrolysis technique and the basic characterizations of the films are mentioned in elsewhere [15]. Additionally, the compositional analysis of two samples was carried out using the X-ray photoelectron spectroscopy (HAXPES beamline). Raman spectra analysis of a sample for confirming the structure was performed using an excitation source of Nd-YAG laser working at a wavelength of 532 nm (LABRAM HR Horiba). The photoluminescence spectra of the films were obtained at room temperature using the JASCO FP-8500 fluorescence spectrometer. Further, Ag electrodes were deposited on the films using silver paste. The current-voltage properties of the samples were studied using a 2636B Keithley dual channel source measurement unit. The relevant electrical parameters of the samples were estimated using the Van der Pauw technique employed in the Keithley 3706A-S Hall card set-up. The photo-response studies were carried out using the Scanning Spectrometer (Model No: HO-SP-SIOOM) detector and a Keithley 2450 source meter. The other parameters of the measurement are given in Table 1. The photo-response measurement set-up is given in Fig. 1.

3. Results and discussion

3.1. Structural characterization

3.1.1. X-ray diffraction studies

The polycrystalline nature of all the $Sn_{1-x}La_xO_2$ (x = 0.01 to 0.10) films was revealed by the X-ray diffraction patterns shown in Fig. 2 (a). The films showed a preferred (1 1 0) plane orientation and the peak positions confirmed the tetragonal phase of SnO_2 upon comparison with the mentioned JCPDS card data. The doping concentration till 10 at. % did not cause for the presence of any impurity peaks within the limit of XRD detection, denoting the successful incorporation of lanthanum ions in the host matrix. The peak intensities were clearly influenced by the amount of La in the host. The obtained average crystallite size of the films varied between ~3 and 12 nm, respectively for 3 and 10 at.% La doped films. The further details of the XRD analysis is available in our previous report [15].

3.1.2. Raman spectra analysis

A typical Raman spectrum of the samples ($Sn_{1-x}La_xO_2$; x = 0.03) is given in Fig. 2 (b) which shows the signature peaks conforming to the tetragonal rutile structure of SnO_2. For detailed information regarding the structural aspects and representation of normal modes of vibration, other sources can be referred [16–18]. In the Raman-active modes of SnO_2, the oxygen atoms vibrate while Sn atoms are at rest, which makes

Table 1
The details of the films and experimental set-up relevant to photoresponse studies.

Illumination range	UVA region
Power	60 mW/cm^2
Bias voltage	9 V
Illumination time	60 s
effective area of exposure	0.6 cm^2
Total area including contacts	1 cm^2
Device type	Planar Metal-Semiconductor-Metal

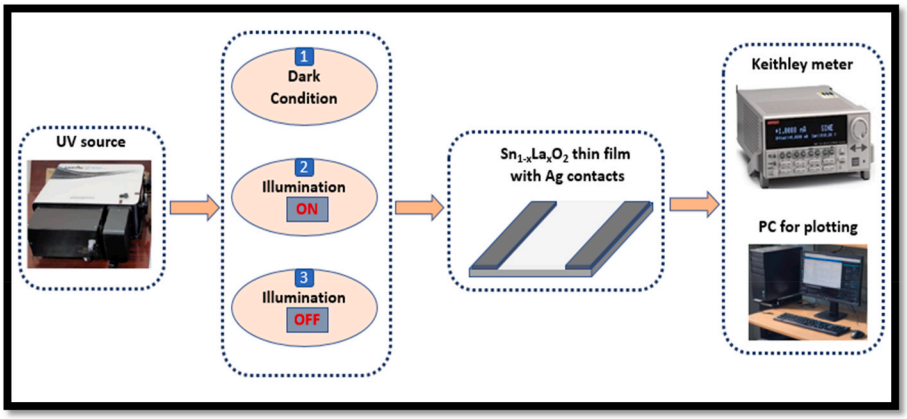

Fig. 1. Schematic diagram of UV photodetection set-up.

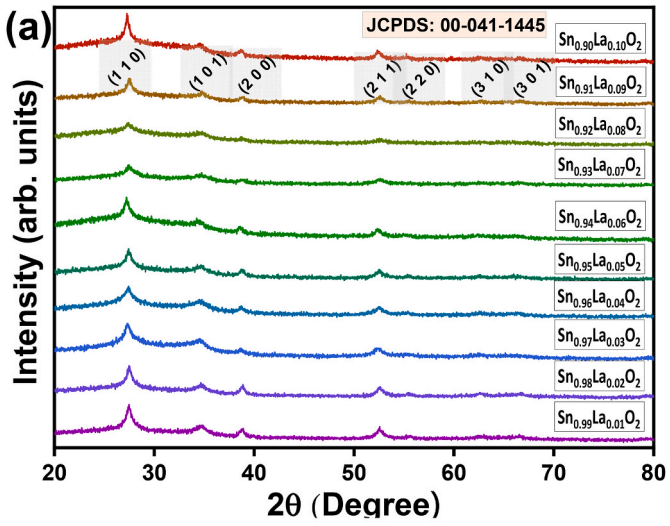

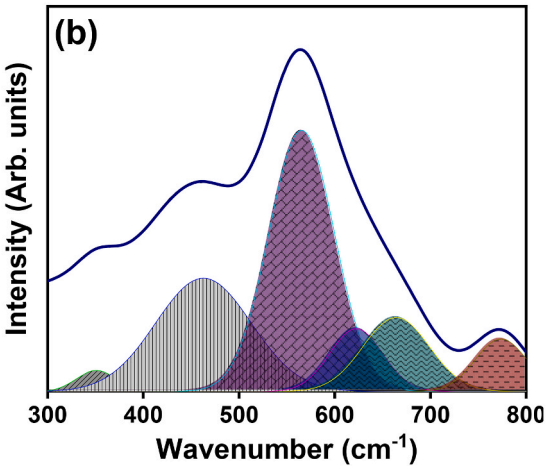

Fig. 2. (a) X-ray diffraction patterns of $Sn_{1-x}La_xO_2$ (x = 0.01 to 0.10) film (b) Raman spectra of $Sn_{1-x}La_xO_2$ (x = 0.03) film.

Raman spectroscopy particularly sensitive to variations in the oxygen sublattice. The broad peaks observed in the Raman spectrum suggest a high density of defects and the confinement of typical crystalline phonon modes within nanocrystals. The broadened peak around ~462 cm^{-1} corresponds to the doubly degenerate mode E_g mode denoting the presence of single ionized oxygen vacancies [19]. Around 622 cm^{-1} peak A_{1g} modes was observed, which is related to the non-degenerate normal phonon modes. Similarly, B_{2g} mode was identified near to 773 cm^{-1} that represented expansion and contraction vibration of the Sn–O bonds. Beyond these signature peaks of bulk SnO_2, the peak observed at 565 cm^{-1} denoted the nanometric dimension of the grains in the samples. The presence of this peak is typically not observed in the spectra of single crystal or polycrystalline SnO_2. This phenomenon is attributed to the influence of surface phonon modes, which become significant, especially when the crystalline size of the material is within the nano regime. In this size range, the substantial surface-to-volume ratio leads to pronounced surface-related effects also [20–23]. Additionally, peak in the range of 350 cm^{-1} and a small peak nearly at 664 cm^{-1} were also visible in the spectra. The relaxation of selection rules or the appearance of Raman forbidden peaks give rise to Raman peaks below 400 cm^{-1} in small particles. In nanocrystalline SnO_2 systems, Raman spectra may display novel modes due to the sensitivity of surface properties to both oxygen vacancies and local disorders. Consequently, the presence of specific modes in the Raman spectra confirmed the nanometric nature of the prepared films.

3.2. Composition and surface morphology features

3.2.1. X-ray photoelectron spectra analysis

In $Sn_{1-x}La_xO_2$ (x = 0.03) film, the XPS survey spectra showed peaks corresponding to the elements tin (Sn), oxygen (O), and lanthanum (La) (Fig. 3 (a)). The Sn 3d peak in the XPS spectrum of the thin films appeared at around 486.3 and 494.7 eV. This peak corresponds to the Sn $3d_{5/2}$ and Sn $3d_{3/2}$ core levels and provides information about the oxidation state of tin, respectively (Fig. 3 (b)). The O 1s peak represents the oxygen atoms in the thin film and provides information about their chemical environment and bonding. In the case of the O 1s peak in the $Sn_{0.97}La_{0.03}O_2$ film, deconvolution can help identify and analyse the different forms in which oxygen is present in the material (Fig. 3 (c)). The contribution to the O 1s peak included lattice oxygen (530.0 eV) and oxygen vacancies (531.6 eV). Additionally, the presence of La^{3+} ions in the thin film was evident from the appearance of La 3d peaks in the XPS spectrum [24,25]. The La 3d peaks were observed at binding energies around 835.0 eV for La $3_{d5/2}$ and 851.4 eV for La $3_{d3/2}$ and confirms the presence of La^{3+} ions in the thin film [24] (Fig. 3 (d)). The survey spectra of $Sn_{0.90}La_{0.10}O_2$ film is also given (Fig. 3 (e)). The signals corresponding to La is more pronounced in the spectra as the La concentration is comparatively very high in this sample. Further, the detailed scan of Sn 3d in the current study shows that the Sn $3d_{5/2}$ and Sn $3d_{3/2}$ peaks were situated at 486.0 and 494.4 eV, respectively, with the indication that Sn existed in a chemical state of '+4' in the sample (Fig. 3 (f)). The two contributions that made up the O1s spectrum, as visible in the deconvoluted spectra for O1s peak, reveals the presence of two different

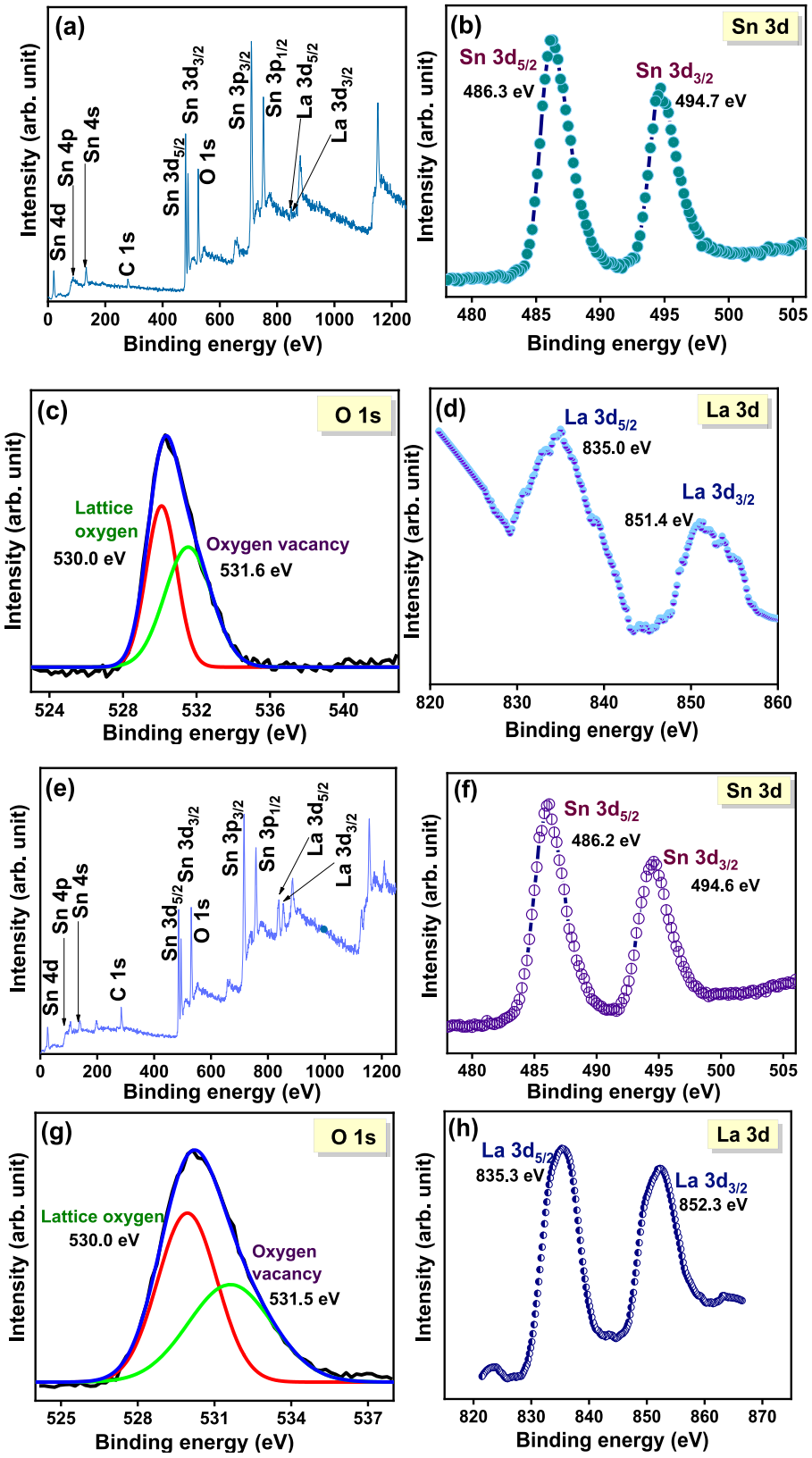

Fig. 3. (a) Survey spectra and detailed scan of (b) Sn 3d (c) O 1s and (d) La 3d of $Sn_{0.97}La_{0.03}O_2$ film; (e) Survey spectra and detailed scan of (f) Sn 3d (g) O 1s and (h) La 3d of $Sn_{0.90}La_{0.10}O_2$ film.

oxygen species in the sample (Fig. 3 (g)). The signal at 530.1 eV was ascribed to the lattice oxygen and that at 531.7 eV to the vacancies of oxygen. The positions of La binding energies are also marked in the respective figures (Fig. 3 (h)). Shi et al. [26] reported that the XPS patterns of La-doped SnO_2 showed signals corresponding to the "+4" valency of tin ion and "+3" valence state of La ion. They reported that these elements existed in the matrix as SnO_2 and La_2O_3. Reports on XPS spectra of spray pyrolyzed La incorporated SnO_2 was also discussed by Wang et al. [27].

The spectra in both cases for Sn3d did not show any peaks corresponding to Sn^{2+} oxidation state. Also, very small shift in the peaks existed. The binding interactions between La-O and Sn-O bonds lead to a charge transfer effect, resulting in a modification of the electronic environment around the Sn^{4+} species. In the Os spectra, the ratio of oxygen vacancy to lattice oxygen (in terms of relative area) was larger in the $Sn_{1-x}La_xO_2$ (x = 0.1) sample than that in the $Sn_{1-x}La_xO_2$ (x = 0.03) sample, showing that the concentration of La changed the distribution of oxygen species in the samples.

3.2.2. SEM micrographs

The SEM images of the $Sn_{1-x}La_xO_2$ films showed clear indication of the influence of la concentration on the surface morphological features of the films (Fig. 4). The microstructures of these films were more or less spherical at lower concentration, whereas, the films grown with higher La ion content exhibited small dispersed particles and loose structures which may be due to the low kinetic energy of the particles in the deposits. Such a morphology for La doped SnO_2 films was not noticed in other related literature. The observed feature of separation of the thin films into small islands gradually resulting in the agglomeration of very small particles into coarser aggregates or patches was nearly similar to the dewetting process [28]. Generally, dewetting arises as a result of the interplay of unfavorable surface interactions and attractive intermolecular forces. The nearly dewetted nature of the present films was unexpected. However, controlled dewetting process can enhance the inherent spatial correlations into a long-range ordering, wherein, objects with a pre-defined statistical size and spatial distribution, can be obtained starting from a homogeneous continuous system, such as a thin film. This leads to the advantage of avoiding complicated and expensive lithographical subtractive processes also. Moreover, there are recent reports on dewetted material components being used in the fabrication of photodetectors [29].

3.3. Photoluminescence spectra and defect distribution

The $Sn_{1-x}La_xO_2$ films were subjected to an excitation of 265 nm (4.67 eV) for studying the influence of La concentration on the PL emission from the films [15]. In SnO_2, oxygen vacancies, tin interstitials or dangling bonds formed during the growth of the films introduce different defect levels within the band gap resulting in different emissions [30]. The observed peaks exhibited different intensities with change in La doping. Generally, the deconvoluted PL spectra consisted of emission signals in the UV, violet, blue, and yellow regions, as reported elsewhere [15]. However, a representative PL emission plot of $Sn_{1-x}La_xO_2$ (x = 0.03 and 0.10) films is shown for reference (Fig. 5 (a)). In this figure, the UV peak at ~359 nm resulted from donor-acceptor recombination (denoted as UV1 in figure). Another UV peak (UV2 in figure) observed around 375 nm was accounted the recombination of deep trapped charges with the photo-generated electrons from the CB. The luminescence centers created by interstitials of Tin produced peak at about 425 nm in the violet range [31]. The decrease of emission intensity due to lanthanide doping can be a consequence of the reduction of crystalline size of the lower concentration La doped films. The emission band at ~460 corresponds to luminescence in blue region which is attributed to different oxygen vacancies [32]. Another peak observed at 573 nm corresponded to yellow emission, which may be due to deeper defect levels or traps existing in the band gap of the films [15].

The estimate of the contribution of different defects in the film to the overall PL signal is shown in Fig. 5 (b). It can be observed that, the changes in the percentage of UV1 emissions were small and rather decreased and increased following the increment in the La concentration, whereas, UV2 showed a reverse trend. It was noticed that the maximum emission in this region was exhibited by the 6 at.% La doped film, which can be considered as a medium level doping in the considered 1 to 10 at. % of La concentration. The violet emission due to tin interstitials also almost followed the trend of UV2. The La^{3+} ions have a "+3" charge state, which can lead to charge compensation effects when introduced into the SnO_2 lattice. This charge compensation can reduce the formation of the typically positively charged tin interstitials. In addition, the incorporation of larger La^{3+} ions at higher concentration can induce more lattice strain, which may energetically discourage the formation of tin interstitials. While, the blue emission resulting from the oxygen vacancies decreased in the medium level doping concentrations. However, the yellow emission did not stick to a monotonic trend among the contributions to the PL signal. The emission peaks at 3.57–3.30 eV (348–375 nm) were ascribed to the shallow donor oxygen vacancy defects by different groups [33–36]. The change of tin interstitials and oxygen vacancies upon La doping was also discussed by Zhang et al. [37] and Boomashri et al. [38]. It is interesting to note that the emission corresponding to the deeper defects and traps in the yellow region is the highest contributor in the list, which can be correlated to the persistence of photocurrent, as discussed in the later sections.

3.4. Electrical characterization

All the $Sn_{1-x}La_xO_2$ (x = 0.01 to 0.1) samples showed linear I-V behaviour with silver contacts (Fig. 6). Here, an unusual behaviour of the nature of slope of the I-V plots could be noticed. A few possible reasons for this are speculated at this point. In the I-V plot, the 1, 2 and 3 at.% La doped films have steeper slopes and the others show very less slope (it also depends on the scale of the plot). Also, the interfaces between the thin film and substrate can significantly affect the transport properties, leading to variations in slope. In the present films a dewetting tendency was observed, which can be considered an interfacial effect due to change in dopant concentration. Another possibility may be changes in grain boundary density which may cause scattering or potential barriers and thereby tend to show non-linear behavior due to carrier-carrier interactions. In the highly doped films, they may be the possibility of scattering due to change in morphology. In addition, doping can modify the surface states of the thin film, it can affect the surface conductivity and possibly lead to variations in the I-V characteristics due to different surface recombination velocities. The surface states and defects act as recombination centers [15], so that if the surface recombination velocity is high, many charge carriers recombine before they can be collected or used, leading to lower output. In thin films, where the surface-to-volume ratio is high, surface recombination can shorten the effective carrier lifetime.

The Hall effect measurement of the samples showed that all the films, regardless of the doping concentration, possessed n-type conductivity. With the increase in the concentration of the dopant in general, the resistivity increased, and carrier concentration dropped, whereas the mobility variation was not monotonous (Table 2). The resistivity was least for 3 at.% while the carrier concentration came up to 3.99×10^{18} cm^{-3} for 6 at.% La doped film. The values of mobility were comparatively higher for lower doping cases (x = 0.01 to 0.03). The absence of a systematic variation in the electrical parameters may be due to the varying degrees of surface features of the films being sensitive to the La concentration. Grain boundary scattering strongly influences the electrical properties. The electrical and optical characteristics of SnO_2 thin films are also influenced by the location of dopants within the matrix. In nanocrystalline systems, dopants exert an effect on the electric properties not only when they occupy regular positions in crystal structures but also when they are distributed over the surface of nanoparticles. Some

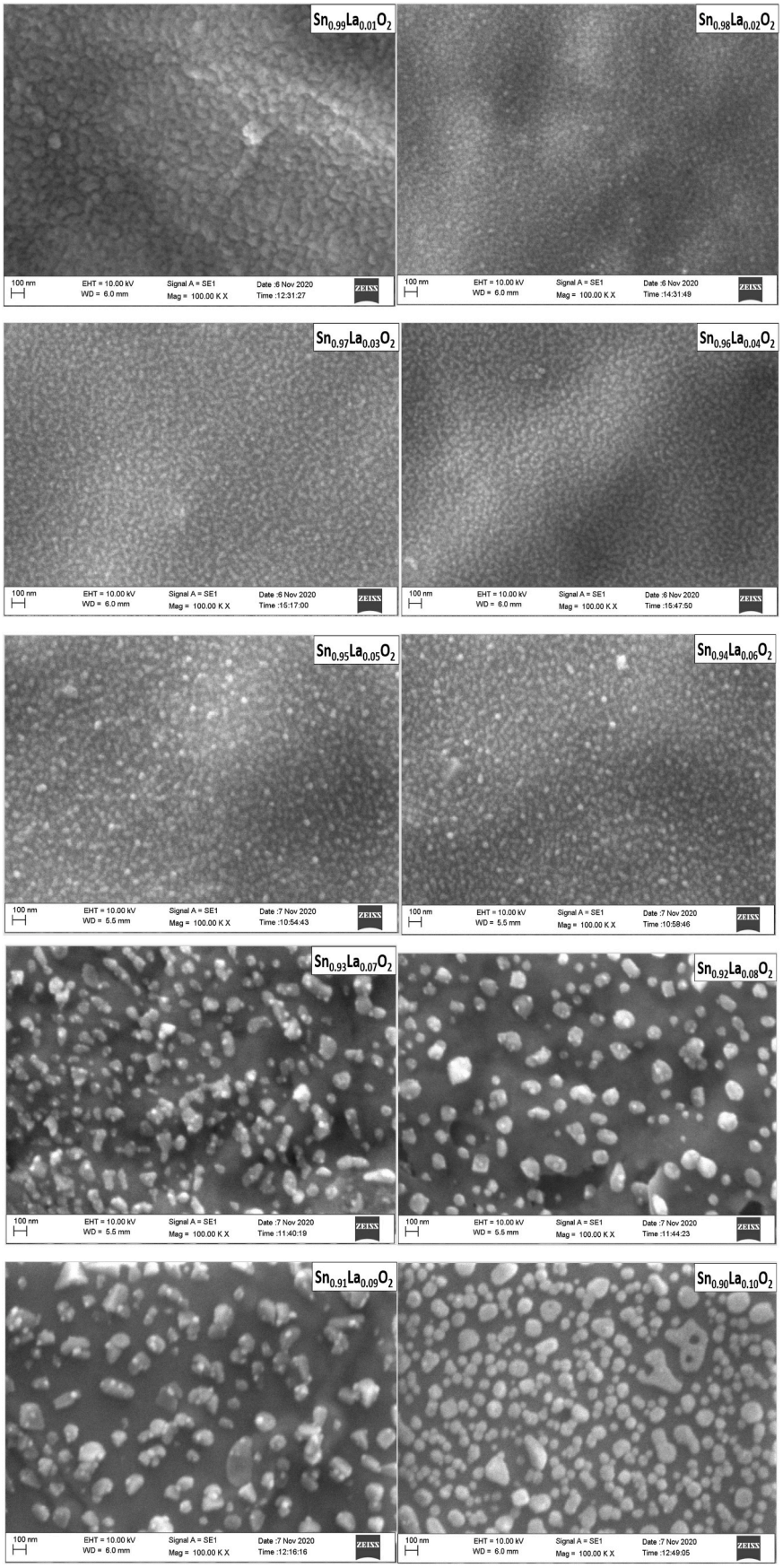

Fig. 4. SEM images of $Sn_{1-x}La_xO_2$ (x = 0.01 to 0.1) films.

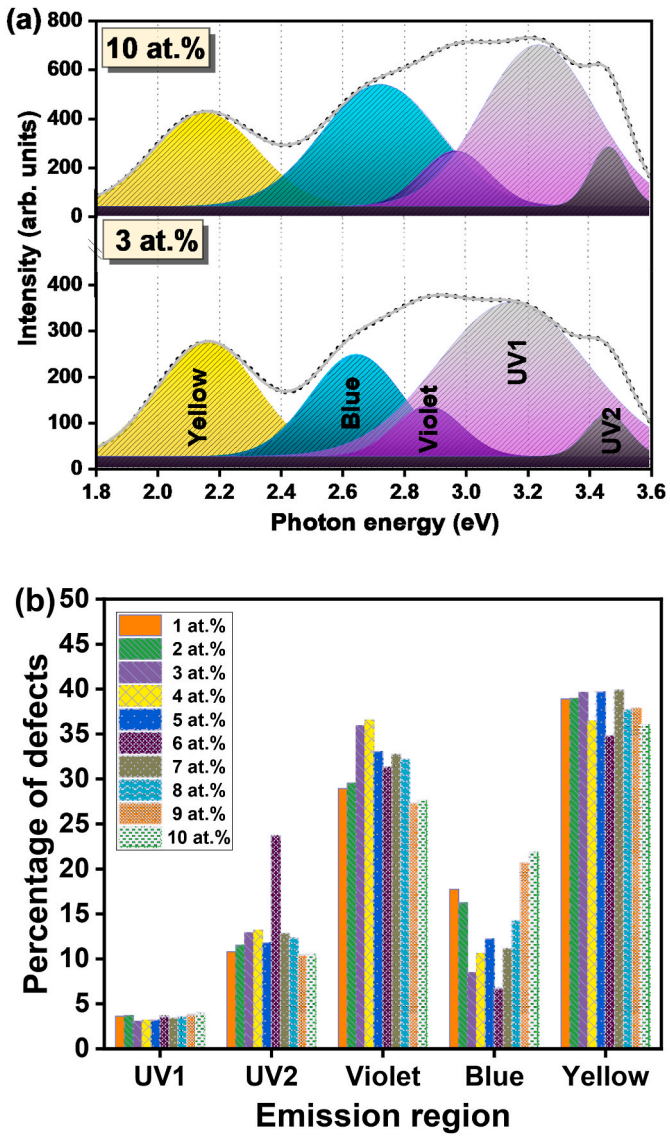

Fig. 5. (a) The deconvoluted PL peaks of $Sn_{1-x}La_xO_2$ (x = 0.03 and 0.10) films and (b) The percentage of defects such as oxygen vacancies present in $Sn_{1-x}La_xO_2$ (x = 0.01 to 0.1) films.

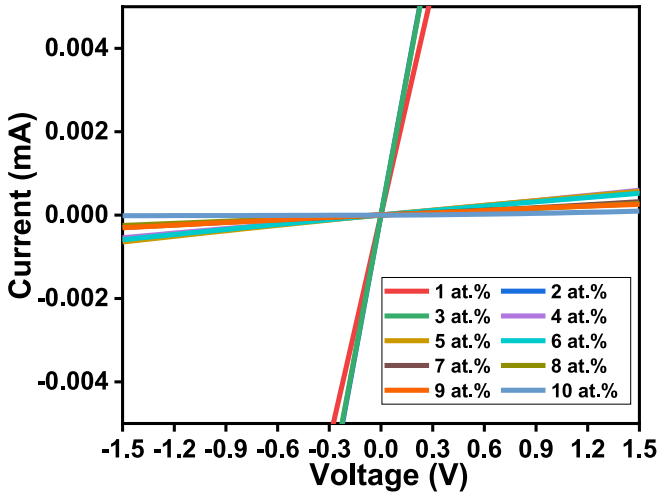

Fig. 6. The I-V characteristics of $Sn_{1-x}La_xO_2$ (x = 0.01 to 0.10) films.

Table 2
Estimation of different electrical parameters of $Sn_{1-x}La_xO_2$ (x = 0 to 0.10) films.

Sample number	Composition	Resistivity (Ω cm)	Mobility cm^2/Vs	Carrier concentration (cm^{-3})
LTO-1	$Sn_{0.99}La_{0.01}O_2$	1.84	36.87	9.19×10^{16}
LTO-2	$Sn_{0.98}La_{0.02}O_2$	42.79	2.30	6.32×10^{16}
LTO-3	$Sn_{0.97}La_{0.03}O_2$	1.30	10.25	4.68×10^{17}
LTO-4	$Sn_{0.96}La_{0.04}O_2$	8.15	1.62	4.70×10^{17}
LTO-5	$Sn_{0.95}La_{0.05}O_2$	16.81	0.90	4.10×10^{17}
LTO-6	$Sn_{0.94}La_{0.06}O_2$	2.65	0.58	3.99×10^{18}
LTO-7	$Sn_{0.93}La_{0.07}O_2$	58.60	0.28	3.68×10^{17}
LTO-8	$Sn_{0.92}La_{0.08}O_2$	2.33	16.57	1.61×10^{17}
LTO-9	$Sn_{0.91}La_{0.09}O_2$	31.80	0.45	4.32×10^{17}
LTO-10	$Sn_{0.90}La_{0.10}O_2$	14.26	0.50	8.74×10^{17}

dopants not only have an effect on the electric properties of SnO_2 but also retard the growth of SnO_2 crystallites and lanthanides are good examples for this. Moreover, in morphological point of view, in metal oxide thin films, sometimes a process called dewetting can occur due to the high surface energy of the films and low adhesion to the substrate. When dewetting occurs, as seen in the morphological features of the films [15], the thin surface area of the film decreases, which leads to an increase in the resistance of the film. It is a process where a thin film breaks apart into isolated droplets due to a lack of adhesion to the substrate or surface tension forces [39]. In earlier studies, it was found that the electrical resistance of the samples increased with an increase in the degree of dewetting [40]. The difference in the behaviour of the conductivity upon doping of nanocrystalline SnO_2 with acceptor impurities can be associated with the difference in the solubility of these dopants in a crystalline matrix in combination with the characteristic features of the formation of impurity states on the nanocrystallite surface [41]. Upon doping La as acceptor in SnO_2, La occupies the Sn site in the matrix such that each La^{3+} ions substitute Sn^{4+} ions and leads to the formation of substituted lanthanum and may introduce oxygen vacancies at the surface. The considerable difference in the ionic radii of these host and dopant ions cause for lattice distortion which can lead to increased electric scattering and reduce the mobility of the carriers, thus increasing resistivity as well [27]. Additives like lanthanum enhance performance and, since the ionic radius of La^{3+} is larger than that of Sn^{4+}, lanthanum preferentially segregates at the grain boundaries. Moreover, La may aid in enhancing adsorption, thereby improving the barrier characteristics at these boundaries [42].

3.5. Photoresponse analysis

Semiconductor photodetectors generate electron-hole pairs when illuminated by photons possessing energies equal to or exceeding their band gap. These pairs can produce a photocurrent when separated by an electric field, which is collected by the electrode of the detector. However, they can show certain properties while they are left in darkness which also contributes to the overall photoconductivity behaviour. In the absence of light, oxygen molecules adsorb onto the SnO_2 film surface, forming ionized oxygen species and a negative charge barrier, contributing to initial dark conductance. Upon UV exposure, electron-hole pairs are generated in the surface of the film, driven by the built-in electric field towards electrodes, enhancing photocurrent. Some attribute this effect to metastable conductive states related to bulk oxygen vacancies, acting as intrinsic doping. UV light desorbs oxygen molecules and generates non-equilibrium carriers, contributing to steady-state photocurrent by reducing surface charge and depletion width.

The photoresponse characteristics of the $Sn_{1-x}La_xO_2$ films upon 1-min illumination with UV light is shown in Fig. 7 (a). Fig. 7 (b) shows the normalized spectra in a short duration for better understanding. It is clear that the nature of the photocurrent shown by the films were sensitive to the La concentration. The dopant concentration influenced

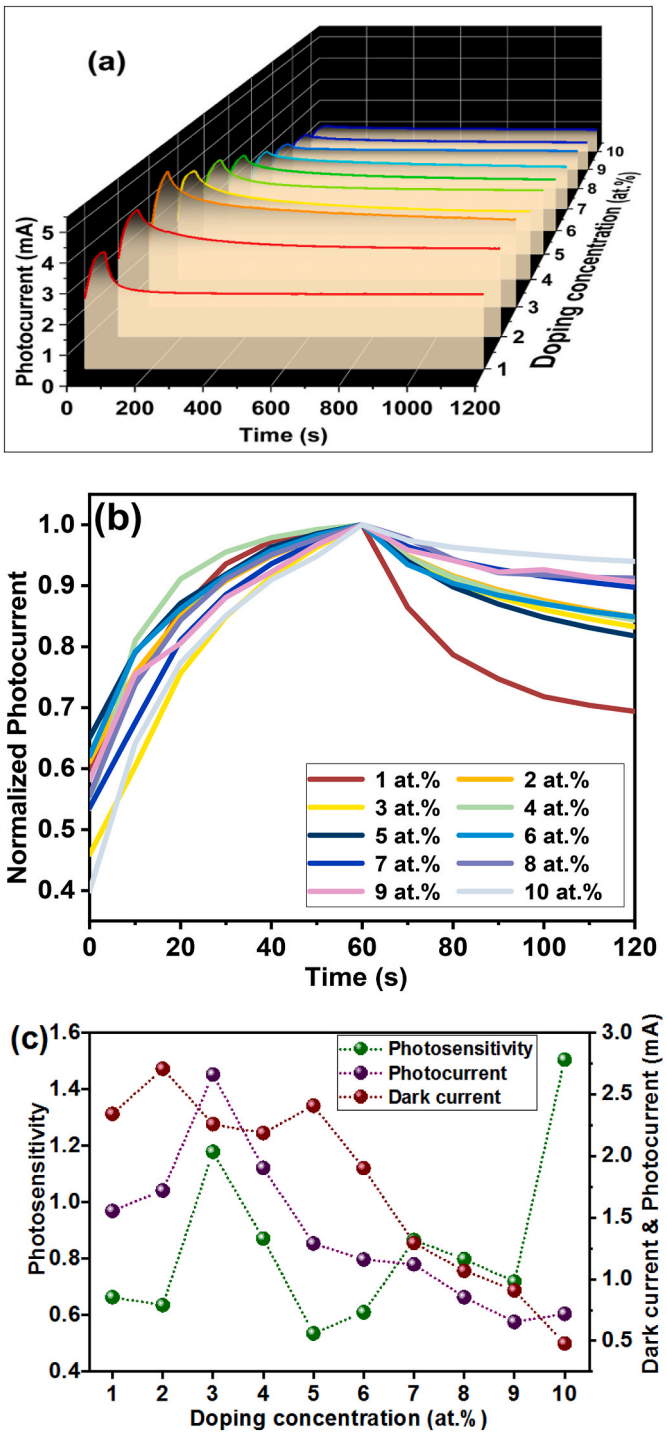

Fig. 7. (a) Variation of photocurrent with time of $Sn_{1-x}La_xO_2$ (x = 0.01 to 0.10) films and (b) Normalized photocurrent transient curves and (c) Dependence of photosensitivity, dark current and photocurrent of $Sn_{1-x}La_xO_2$ (x = 0.01 to 0.10) films on doping concentration of La.

many key parameters involved such as the dark current, the time taken for the rise of photocurrent, extent of photocurrent, the time taken for the fall of the photocurrent and the decay behaviour. A general decreasing trend of dark current with the increase in La content could be observed, and rather similar trend was exhibited by the amount of maximum photocurrent reached during the illumination (Fig. 7 (c)). Fig. 7 (c) also shows the variation of photocurrent (difference between the maximum current reached at illumination and the initial dark current) and photosensitivity (the ratio between photocurrent and dark current) of the films according to the change in La concentration. The photocurrent and photosensitivity initially increased till 3 at. % of La doping, decreased in the case of medium level of doping. The highest photocurrent was achieved at a doping level of 3 at.% (2.66 mA), which was the film with the least crystallite size. However, the trend changes thereafter, in the case of the photocurrent it further decreased with increase in La concentration, whereas the photosensitivity rather followed a general increasing trend, peaking at 10 at.% with a value of 1.5. This anomalous behaviour can be linked to the unsystematic variations exhibited by the electrical parameters by virtue of their different surface features and trade-off between different defect concentrations. The doping can modify the energy levels and band structure of the material, creating favourable conditions for efficient charge separation and transport. The introduction of dopant atoms can shift the energy levels, create trap states, or alter the bandgap, leading to enhanced photoinduced charge transfer processes and improved photoresponse [43]. A higher photosensitivity allows for more precise data recording in optical memory devices, while a lower sensitivity can result in errors and reduced data density. Similar observation related to the crystallite size and speed of photoresponse was made by Ghosh et al. [44]. According to them, a faster photoresponse decay was observed in the film with smaller crystallite size with porous microstructure.

The rise times of the different films, defined as the time required for the photocurrent to rise from 10 % to 90 % of the maximum photocurrent, are given in Table 3. Here, interestingly, it can be observed that as the concentration of La in the matrix increased, the rise time initially increased till 3 at.% and then decreased, showing an overall minimum at 6 at.%. At higher concentrations also the rise time showed an increasing trend. That is, The 3 at. % and 10 at. % showed more time to increase the photocurrent to its peak at the 60th second of illumination. The rise time denotes the time taken for the filling of carriers, while the decay time corresponds to the time taken for the release of carriers from the traps. A fast rise time response can be attributed to the dominant rapid process of photogeneration of electron-hole pairs. Depending on the doping level and the resulting changes in carrier dynamics, the rise time may be influenced through alterations in carrier transit times and recombination rates. The introduction of dopant ions led to shifts in the absorption edge and changes in the energy band gap of the material [15]. As observed, doping with La^{3+} ions enhanced the defect states and trap levels within the tin oxide lattice. The density and distribution of these defects can influence carrier recombination processes and charge transport mechanisms, thereby affecting the rise time of the photodetector.

When the UV source was removed, electron–hole recombination process dominated, and thus the conductivity started to diminish, whose speed depended on different factors indirectly connected with the change in La concentration. The fall time (time taken by the photocurrent to drop from maximum to 10 % of the maximum photocurrent) could not be identified with in the present experimental conditions for all the samples except 1 and 5 at.% la doped films (~609 and 794 s, respectively). The decay behaviour of the films was interesting as considerable differences could be noticed in the way the photocurrent decayed once the illumination was turned off. A few observations came into picture here. The decay curves showed initial sudden decrease to a certain level of photocurrent and then followed slow or very slow decay and did not come back to the initial dark current value. The decay curves can be suitably fitted to perceive more information about the reasons for the undergoing relaxation processes.

Most of the works on PPC of tin oxide reported decay curve fitting using stretched exponential. For example, Brinzari [7] interpreted the stretched exponential behaviour exhibited by the decay of photoconductivity in terms of the structural and electronic disorder in the film, which results in an asymmetric probability distribution of inter-grain barrier heights and the distribution of the associated time constants. Generally, stretched exponential decay occurs more rapidly than ordinary exponential decay. Similarly, Viana et al. [5], Tierney et al. [6] and

Table 3
The rise time, relaxation time constants and percentage of photocurrent retention of $Sn_{1-x}La_xO_2$ (x = 0.01 to 0.10) films.

Sample number	Composition	Rise time (s)	Relaxation time (s)			Percentage of photocurrent retained after 10^4 s (Theoretical)
			τ_1	τ_2	τ_3	
LTO-1	$Sn_{0.99}La_{0.01}O_2$	32.5	52.09	14.44	249.96	9.2 %
LTO-2	$Sn_{0.98}La_{0.02}O_2$	41.5	20.11	161.01	540.93	18.2 %
LTO-3	$Sn_{0.97}La_{0.03}O_2$	42.83	15.25	78.41	913.38	24.3 %
LTO-4	$Sn_{0.96}La_{0.04}O_2$	38.92	12.01	86.53	503.36	16.4 %
LTO-5	$Sn_{0.95}La_{0.05}O_2$	34.58	19.38	81.58	435.92	5.5 %
LTO-6	$Sn_{0.94}La_{0.06}O_2$	23.96	12.91	59.74	432.21	10.8 %
LTO-7	$Sn_{0.93}La_{0.07}O_2$	39.98	14.65	83.62	911.72	30.6 %
LTO-8	$Sn_{0.92}La_{0.08}O_2$	38.32	27.16	720.23	–	63.1 %
LTO-9	$Sn_{0.91}La_{0.09}O_2$	42.29	6.92	74.92	622.90	41.1 %
LTO-10	$Sn_{0.90}La_{0.10}O_2$	44.17	75.79	1375.82	–	63.8 %

Costa et al. [8] performed decay fitting using stretched exponential decay function, whereas, in Al doped SnO_2 thin films, Selma et al. [45] obtained photocurrent decay curve that fitted to a bi-exponential function with time constants representing a fast and a slow photocurrent decay. They attributed the fast decaying to the recombination of photogenerated electron–hole pairs, and the slow decrease to the re-adsorption process. In the present case, however, the situation was different. A satisfactory fit required at least three exponential components for all the films except 8 at.% and 10 at.% doped ones. The best fit for the photocurrent decay curves of $Sn_{1-x}La_xO_2$ films was obtained using the functions given by:

$$I(t) = I_0 + \alpha_1 e^{\left[-\left(t/\tau_1\right)\right]} + \alpha_2 e^{\left[-\left(t/\tau_2\right)\right]} \quad (1)$$

$$I(t) = I_0 + \alpha_1 e^{\left[-\left(t/\tau_1\right)\right]} + \alpha_2 e^{\left[-\left(t/\tau_2\right)\right]} + \alpha_3 e^{\left[-\left(t/\tau_3\right)\right]} \quad (2)$$

Here, I_0 is the y-offset, the decay time constants are τ_1, τ_2, τ_3 and α_1, α_2, α_3, denotes the pre-exponential factors. The decay time constants respectively represent ultrafast, fast and slow decay process undergone by the carriers (Table 3). The ultrafast decay component represents the result of the recombination from surface defect states while the slow process may be the result of band to band recombination or a donor-acceptor pair recombination [46]. The slow decay may also be influenced by spatially separated trapped carriers, which delay the recombination due to the presence of potential barrier. The third component may be related to the additional trapping centers [47]. In La doped SnO_2 used as electron transport layer for planar hybrid perovskite solar cells as reported by Xu et al. [25], time resolved PL spectra revealed bi-exponential decay parameters, where the fast component indicated defect trapping and the slow component was accounted for the recombination life time. They observed that upon La doping, the average lifetime reduced.

It is worth noting that, all of the $Sn_{1-x}La_xO_2$ films, irrespective of their dopant concentration, showed certain level of persistent photocurrent, wherein most of the cases, the films took more than 1200s to come to at least half of the initial dark current value. The presence of defects like oxygen vacancies and tin interstitials were already evident from the PL data. The oxygen vacancies can act as trap states for electrons or holes in the material. Upon the termination of UV exposure, majority of the electrons present in the CB recombine with the corresponding holes in the VB. The remaining get deeply trapped at the recombination centers, giving rise to PPC.

In SnO_2, the n-type semiconducting nature originates from the oxygen vacancies formed from the escape of O^{2-} ions from crystal lattice site. These vacancies occur when oxygen atoms are missing from their regular lattice sites, leaving behind free electrons in the conduction band. The missing oxygen atom creates a defect state in the crystal. This defect state corresponds to an energy level that lies within the bandgap between the valence and conduction bands. These defect states are often referred to as donor levels because they can donate electrons to the conduction band. The presence of these defect states means that the material can absorb photons with energies lower than the actual bandgap of SnO_2. Due to this, less energy is required to excite an electron from the defect state to the conduction band [48].

Each oxygen vacancy typically donates two electrons to the conduction band. The stabilization of oxygen vacancy defects takes place by charge compensation mechanisms. They can either donate or capture up to two electrons which characterizes them as electron traps. Neutral vacancies, $V_o^{\,0}$, can donate up to two electrons, while, $V_o^{\,\bullet}$ are donors or capture only one electron, whereas, $V_o^{\,\bullet\bullet}$ cannot donate electrons but can capture up to two electrons. These trap centers are related by the following equations [8]: $V_o^{\,0} \leftrightarrow V_o^{\,\bullet} + e^-$ and $V_o^{\,\bullet} \leftrightarrow V_o^{\,\bullet\bullet} + 2e^-$. Upon La doping, La^{3+} replaces Sn^{4+} in the SnO_2 lattice and La^{3+} has one positive charge less than Sn^{4+}. Each La^{3+} substitution make electrons to be liberated from oxygen vacancies to balance the reduced positive charge at the La^{3+} substitution sites for the purpose of maintaining charge neutrality. This additional electron does not remain bound at the La^{3+} site but becomes a free electron in the CB and increases the number of free charge carriers in the CB, thus enhancing the n-type character of the material. This is also supported by the carrier concentration of the $Sn_{1-x}La_xO_2$ films obtained from the electrical characterization [49].

At low La^{3+} concentrations, introducing La^{3+} creates isolated substitution sites, where the La^{3+} ions replace Sn^{4+} ions. As mentioned, the charge imbalance can be compensated by existing or newly created oxygen vacancies. In this case, the La doping can increase the number of oxygen vacancies, as the lattice tries to maintain charge neutrality by generating these vacancies. The increased oxygen vacancy concentration in La doped SnO_2 leads to enhanced PL emission, particularly in the blue and yellow regions, which are associated with neutral and singly ionized oxygen vacancies. However, the PL data showed that, the blue emission attributed to oxygen vacancy showed a decreasing tendency till medium level of doping. Here, another possibility may be that oxygen vacancies can also lead to PL quenching, that is, a reduction in PL intensity due to them acting as non-radiative recombination centers, where excited electrons recombine with holes without photon emission [50]. This non-radiative recombination can occur if there is a very high concentration of oxygen vacancies or if they act as trapping centers that hinder radiative recombination. This may be one reason for the general decreasing PL intensity observed for the blue emission at medium level doping. Moreover, the yellow emission involving traps can be speculated to be also due to doubly ionized oxygen vacancy as this defect state is typically deeper in the band gap compared to the singly ionized vacancy. Electrons trapped in these deeper levels are less likely to be excited into the conduction band at room temperature, and the defect acts as a much deeper donor. As it can be observed from the PL data, the influence of signal from this emission has significantly contributed to the overall photoluminescence intensity [51,52]. Whereas, at higher doping levels, oxygen atoms are more likely to leave their lattice positions, creating vacancies, especially at the surface, due to the already weakened bonds there. However, at such doping levels, the material may

reach a saturation point, where additional La^{3+} doping may not further increase conductivity because of the formation of fewer oxygen vacancies and quenching, or the material becomes too heavily doped, leading to possibilities of electron scattering or other defects that can decrease mobility [53–55].

It also follows from the result of optical characterization wherein, the Urbach energy was observed to be more in higher La doped samples, peaking at 984 meV for 10 at.% La doped sample [15]. Further, it is known that the Urbach energy is related to the density of localized states within the bandgap. Higher Urbach energies generally indicate a higher density of localized states and increased disorder in the material. That is, the number of electronic energy levels or states within the bandgap of a material is more in samples with more La ions. These localized states can trap and influence the movement of charge carriers in the material [56]. When the photogenerated charge carriers are trapped in these states, the recombination is further delayed. Hence, one major reason for the high amount of persistence shown by the $Sn_{0.90}La_{0.10}O_2$ film is the high value of Urbach energy of the films. The PPC phenomena is also dependent on the surface properties of materials, especially in nanomaterial-based devices with a large surface-to-volume ratio, where the spontaneous surface potential spatially separates the photogenerated electron-hole pairs. Consequently, after the cessation of the photoexcitation, these nonequilibrium carriers can continue to cycle across the transport channel for an extended period of time before recombining, resulting in persistent photocurrent.

Moreover, the surface oxygen vacancies can also contribute to the PL signal. Since SnO_2 is often used in nanostructured or nanoparticle forms (where surface-to-volume ratios are high), surface oxygen vacancies can dominate the photoluminescence properties. The PL from surface vacancies may differ slightly in energy from that of bulk vacancies due to changes in the local environment at the surface. At the surface, oxygen atoms are more loosely bound compared to atoms in the bulk because they have fewer neighbouring atoms to bond with. This makes surface oxygen atoms more susceptible to removal, when oxygen atoms leave the surface, they create oxygen vacancies, which are essentially surface defects. These vacancies can lead to dangling bonds or under-coordinated surface atoms, which significantly alter the material's electronic properties. The surface oxygen vacancies contribute free electrons to the material, just like bulk vacancies, enhancing n-type conductivity. The electrons released from these vacancies can increase the surface conductivity, which is particularly important for thin films or nanostructures where surface-to-volume ratios are high. Surface oxygen vacancies make the material more chemically reactive because they provide sites where adsorbates (like oxygen, water, or gas molecules) can easily bond. Moreover, oxygen vacancies on the surface act as active sites for the adsorption of molecules like oxygen (O_2), which can also influence photoresponse [57,58].

The oxygen vacancies can also lead to surface reconstruction, a process where the arrangement of atoms at the surface changes to minimize energy. This can result in the creation of new surface defect structures also [59,60]. Besides, for higher doping concentrations in the prepared films, as mentioned in SEM analysis, a property similar to dewetting has been observed. Generally, dewetted surfaces refer to a morphology where the film has pulled back resulting in fewer grain boundaries compared to a film with small, closely packed grains-the films with lower doping level in the present case. While there may be some grain boundaries within the islands themselves, the overall connectivity and number of interfaces may be lower compared to a film with uniformly small grains [40]. At higher concentrations, the dopant can induce stress or phase separation in the SnO_2 matrix, leading to a tendency for the film to dewet. If the doping level is too high, it can disrupt the continuity of the film and lead to the formation of islands as the material tend to pull away from the substrate. Such nearly dewetted morphology in the present $Sn_{1-x}La_xO_2$ (x = 0.07 to 0.10) films influence their electrical properties. As, dewetted films often consist of isolated islands or droplets, leading to reduced continuous pathways for charge carrier transport. This lack of connectivity can significantly lower the electrical conductivity of the film, which was observed in the electrical properties of these highly doped films. Also, the presence of interfaces and boundaries in dewetted regions can scatter charge carriers, further decreasing their mobility. The presence of a dewetted morphology can create additional surface states or defects at the edges of islands which can trap charge carriers, reducing the available charge for conduction. The accumulation of trapped charges can lead to increased resistance in the film also. However, dewetting may be advantageous for delayed photocurrent decay in charge storage applications the introduction of additional surface states that trap charge carriers can prolong the lifetime of the photogenerated carriers, leading to a delayed photocurrent decay. The formation of islands or droplets is likely to increase the surface area of the film which can provide more active sites for light absorption and charge collection, enhancing the photosensitivity and allowing for more effective charge storage. In dewetted structures, the isolation of charge carriers due to physical separation, charge trapping, reduced mobility, and localized fields all contribute to lower recombination rates, which extends the lifetime of photogenerated carriers. This leads to a delayed photocurrent decay and enhances the ability of the films to store and utilize charge over longer periods, which is particularly beneficial in memory storage devices. However, achieving an optimal balance between the benefits of dewetted morphology and the challenges it presents is crucial for maximizing performance in practical applications.

The decay time of persistent photocurrent (or retention time as in the case of memory elements) is one of the most important criteria required for sustaining information for a long period of time in a non-volatile manner [10]. To further examine the viability of the prepared $Sn_{1-x}La_xO_2$ films for long-term persistence, the theoretical extrapolation of the obtained transient photocurrent curves beyond the experimental duration 1200 s to 10,000 s was performed (Fig. 8 (a). It can be observed that even after ~2.7 h most of the films are showing considerable persistent photocurrent, ie, some amount of current is retained in these films after a long time since the removal of the UV source. For better understanding of the situation, the percentage of photocurrent retained after 10000 s estimated as per the theoretical extrapolation of the decay curve was calculated (Table 3). The $Sn_{1-x}La_xO_2$ films with La doping concentrations near to 10 at.% showed more amount of retained photocurrent, with 10 at.% La doped film possessing a maximum of nearly 64 % of retention, which means that, more than 50 % of the photocurrent can be stored for a long time in future. This marks the suitability $Sn_{1-x}La_xO_2$ of these films for memory applications.

Unfortunately, there are not many reports that give stress on the importance of doping in the photoconductivity studies pertaining to PPC, especially in binary metal oxides that pay attention to the different experimental parameters involved. In a theoretical study based on the of photoconductivity decay in Sb doped SnO_2 thin films Floriano et al. [61] suggested that compared to the Sb doped SnO_2 with rare earth doped SnO_2 thin films, the recombination process was found to be much energy-consuming in the rare earth doped compound, as dopant ions like Er^{3+} and Eu^{3+} behave as acceptors in such materials and also have deeper energy levels. Selma et al. [45] observed that both the dark current and photocurrent decreased with increase in Al concentration in the case of Aluminium doped SnO_2 thin films. The study on photo-response of Al doped ZnO multilayered thin films by Ganesh et al. [62] revealed increase in the photocurrent upon doping, where the photocurrent reached its peak value, nearly 50 times higher than the dark current, in the case of 1.5 wt% Al doped ZnO. The photocurrent decreased with further increase in Al doping, similar to that of the trend observed in the present study. The rise time was shorter for the 1.5 wt% Al doped films compared to other doped films but was, however, longer than that of undoped ZnO.

In literature a few reports are available on the applicability of persistent photoconductivity phenomenon in optical memory elements with three or two terminal devices. For example, Sun et al. [9] fabricated

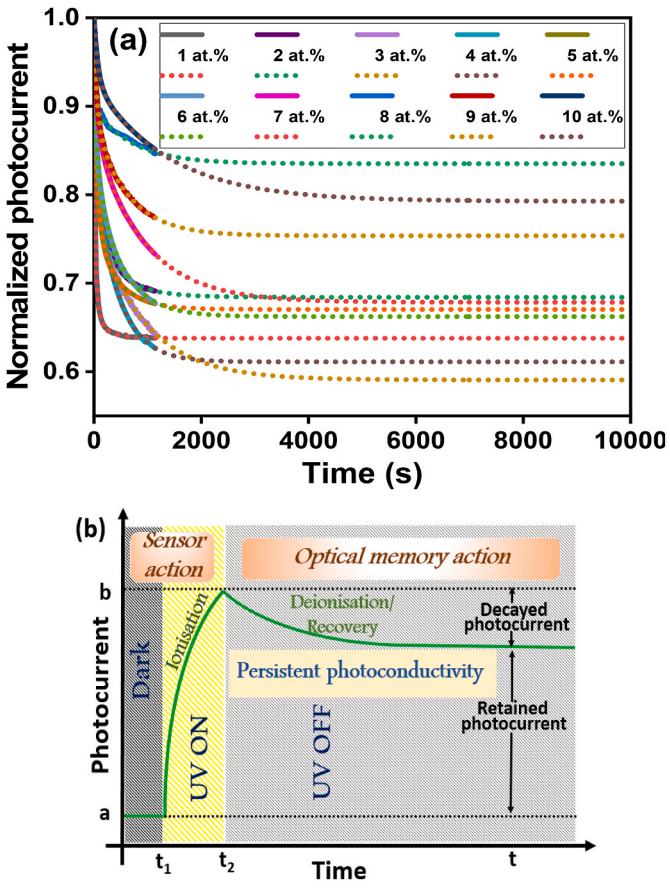

Fig. 8. (a) The normalized photocurrent vs. time graph of $Sn_{1-x}La_xO_2$ (x = 0.01 to 0.10) thin films theoretically fitted using suitable exponential functions and extrapolated to 10000 s after the removal of UV source (b) Representation of different attributes of a typical material exhibiting persistent photoconduction suitable for optical memory; 'a' and 'b' denotes the dark current and maximum current obtained during illumination, respectively; t_1 and t_2 corresponds to the time of beginning and cessation of UV illumination and t denotes time at any instant of measurement of other related parameters.

a reconfigurable optical memory device using a MoS_2/quantum dots mixed-dimensional heterostructure with photonic programming and electric erasing capabilities. They observed a unique photoelectric coupling effect between MoS_2 and QDs, wherein light exposure resulted in continuous n-doping of the MoS_2 channel even after exposure ceased, leading to the generation of PPC. Similarly, Dai et al. [10] demonstrated phototransistors featuring a large photo-to-dark current ratio and long-lasting PPC using a nanocomposite of amorphous indium-gallium-zinc oxide and graphene nanosheets synthesized via a sol-gel technique. This long-lasting photocurrent with lifetime up to years in the device can be used in applications including optical memory due to its ability to precisely control the ON and OFF states. Also, report from Gadelha et al. [11] demonstrated the possibility of obtaining a non-volatile photomemory effect with high ON/OFF ratio in a field effect transistor architecture with high doping values achieved with laser exposure. The binary photomemory was generated by virtue of PPC effect pertaining to long memory retention time. Fortunately, this application is not limited to complicated device configurations only. For instance, Abbas et al. [12] reported photomemory of In_2O_3 thin films prepared using sputtering method on glass and PET substrate that revealed greater than 10^4 s of persistence, capable of retaining optical information at room temperature. They also analysed PPC for multibit data storage by programming with intensity, photon pulse etc. Dixit et al. [13] observed long lasting PPC in Au coated CuO thin films suitable for non-volatile optical memory application. The SET and RESET processes were established using optical excitation using deep UV illumination and NIR excitation, respectively. Lee et al. [14] suggested that the giant PPC observed in VO_2 thin film device prepared on corning glass can contribute to realizing the optical remote controlling of electronic devices like optical memories.

The summary of the features of a typical transient photoresponse of a material showing PPC behaviour under different conditions under suitable bias suitable for memory action is shown as a schematic diagram in Fig. 8 (b). It shows three regions based on the condition of illuminations, viz, (i) the initial dark condition where illumination is absent (ii) the duration of illumination and (iii) the condition after the illumination is removed. The responses are the stabilization of dark current (not necessarily included in some graphs), the emergence and rise of photocurrent and thirdly, the decay of the photocurrent, respectively. The first two regions correspond to the sensor action, wherein the advent of the UV illumination is detected in the form of proportionate increase in the photocurrent. Ionization occurs during this phase. Further, the decay phase represents the optical memory action, where the deionization occurs leading to the recovery of the condition under dark. Further, there are several crucial factors for achieving significant PPC. First, the transport channel materials must be optically active and capable of efficiently converting incident photons into photogenerated electron-hole pairs when exposed to light. Second, a spontaneous built-in electric field is necessary to spatially separate these photogenerated electron-hole pairs, preventing their rapid recombination. Lastly, there should be numerous localized defect states that trap one type of photogenerated carrier, allowing the other type to participate freely in the transport process [63]. Thus, the information can be stored in the form of current states using an input light pulse. Such a system can be easily programmed with an external bias voltage, by varying the intensity, and adjusting the chopping frequency of light, creating a non-volatile multilevel storage system. Interestingly, it can be observed from the obtained results that these criteria, along with long-lasting PPC are met by the present $Sn_{1-x}La_xO_2$ films in varying degrees based on the amount of La ions incorporated in them. Hence, the observed long-lasting persistent photocurrent in the present $Sn_{1-x}La_xO_2$ films especially in the higher doping cases can be extended for utilization in optical memory components and related devices.

4. Conclusion

To summarize, this study investigated the structural, optical and electrical properties of $Sn_{1-x}La_xO_2$ (x = 0.01 to 0.1) films deposited on glass substrates, deposited via spray pyrolysis, focusing on impact of lanthanum concentration on the photoresponse characteristics of the films. In the Raman spectra of $Sn_{1-x}La_xO_2$ (x = 0.03) film, the peaks indicating oxygen vacancies and nanometric grain size were present along with the typical Raman active modes of tin oxide. The XPS spectra revealed the Sn^{4+} and La^{3+} states of tin and lanthanum and the contribution of lattice oxygen and oxygen vacancy in the films. The photoluminescence emissions exhibited by the $Sn_{1-x}La_xO_2$ films varied with La concentration and showed signals in the UV, violet blue and yellow wavelength regions corresponding to tin interstitials, oxygen vacancies and other defects present in the films. All the $Sn_{1-x}La_xO_2$ films indicated n-type conductivity, with La concentration influencing the resistivity and carrier concentration of the films. The silver electrodes rendered Ohmic contacts in the films, as revealed in the linear I-V characteristics of the films. The photoconductivity studies showed that UV exposure enhanced the photocurrent exhibited by the films, influenced by La doping which affected energy levels and defect states. The photocurrent and photosensitivity trend varied with La concentration, and the photocurrent decay behaviour of most of the films showed a need for tri-exponential fitting indicating different decay time constants. The increase in the La concentration in the films slowed down the photocurrent decay process extending to hours. Thus, the long-lasting persistent photocurrent observed in the films with higher La doping concentration

makes these films suitable for optical memory components and related devices.

CRediT authorship contribution statement

P. Asha Hind: Writing – original draft, Visualization, Validation, Software, Formal analysis, Data curation. **Pawan Kumar:** Validation, Software, Investigation, Formal analysis. **U.K. Goutam:** Validation, Supervision, Software, Resources. **B.V. Rajendra:** Writing – review & editing, Supervision, Project administration, Methodology, Investigation, Funding acquisition, Conceptualization.

Novelty statement

Following important observation noticed during our experiment on La doped SnO_2 thin films.

- Fabricated simple planar MSM structured films suitable for non-volatile memory retention applications
- Variation of oxygen vacancies in the deposits with dopant level influenced the photoconductivity
- Higher dopant concentration in the films retained more photocurrent
- Long lasting persistent photoconductivity after removal of UV exposure.
- Tunability of photocurrent decay time through La doping
- These features are suitable for optical memory applications

Declaration of Competing Interest

The authors declare that they have no known competing financial interests or personal relationships that could have appeared to influence the work reported in this paper.

Acknowledgement

The authors express their gratitude to Manipal Academy of Higher Education, Manipal, for providing the basic infrastructure and advanced characterization facilities. Authors are grateful to RRCAT Indore center for the XPS facility. This work was also partially supported by UGC-DAE CSR, Mumbai Center, India through project no. UDCSR/MUM/AO/CRS-M-315/2020/352. MAHE Manipal-UNSW Sydney Australia sanctioning seed fund aided for collaborative research work. Central Sophisticated Instrumentation facility of BITS, Pilani Goa Campus is also thanked for helping in carry out the Raman spectroscopy measurements. The authors are also indebted to Dr. Gowrish Rao, Dr. Mahesha M G and their doctoral students for facilitating the set-ups for photoresponse studies. The authors are grateful to Dr. Sudha. D. Kamath for helping to conduct photoluminescence characterization in her laboratory.

Data availability

Data will be made available on request.

References

[1] C.F. Bueno, Transient Decay of Photoinduced Current in semiconductors and heterostructures, 2020.
[2] C.I. Bright, Transparent conductive thin films, Elsevier LTD., 2018, https://doi.org/10.1016/B978-0-08-102073-9.00021-7.
[3] S. Das, V. Jayaraman, SnO2: a comprehensive review on structures and gas sensors, Prog. Mater. Sci. 66 (2014) 112–255, https://doi.org/10.1016/j.pmatsci.2014.06.003.
[4] D. Tsoutsou, G. Scarel, A. Debernardi, S.C. Capelli, S.N. Volkos, L. Lamagna, S. Schamm, P.-E. Coulon, M. Fanciulli, Infrared spectroscopy and X-ray diffraction studies on the crystallographic evolution of La2O3 films upon annealing, Microelectron. Eng. 85 (2008) 2411–2413.
[5] E.R. Viana, J.C. González, G.M. Ribeiro, A.G. De Oliveira, Photoluminescence and high-temperature persistent photoconductivity experiments in SnO2 nanobelts, J. Phys. Chem. C 117 (2013) 7844–7849, https://doi.org/10.1021/jp312191c.
[6] P. Tierney, T.J. Ennis, Á. Allen, J. Wright, The role of mid-band gap defect levels in persistent photoconductivity in RF sputtered SnO 2 thin fi lms, Thin Solid Films 603 (2016) 50–55, https://doi.org/10.1016/j.tsf.2015.12.058.
[7] V. Brinzari, Mechanism of band gap persistent photoconductivity (PPC) in SnO 2 nanoscrystalline filmsNature of local states, simulation of PPC and comparison with experiment, Appl. Surf. Sci. 411 (2017) 437–448, https://doi.org/10.1016/j.apsusc.2017.03.209.
[8] I.M. Costa, M.D. Teodoro, M.A. Zaghete, A.J. Chiquito, Influence of the metastable state (V 0++) on the electronic properties of SnO2nanowires under the influence of light, J. Appl. Phys. 128 (2020), https://doi.org/10.1063/5.0021719, 0–9.
[9] Y. Sun, Y. Ding, D. Xie, M. Sun, J. Xu, P. Yang, Y. Zhang, T. Ren, Reconfigurable optical memory based on MoS2/QDs mixed-dimensional van der Waals heterostructure, 2D Mater. 8 (2021) 25021.
[10] M.-K. Dai, Y.-R. Liou, J.-T. Lian, T.-Y. Lin, Y.-F. Chen, Multifunctionality of giant and long-lasting persistent photoconductivity: semiconductor–conductor transition in graphene nanosheets and amorphous InGaZnO hybrids, Acs Photonics 2 (2015) 1057–1064.
[11] A.C. Gadelha, A.R. Cadore, K. Watanabe, T. Taniguchi, A.M. de Paula, L.M. Malard, R.G. Lacerda, L.C. Campos, Gate-tunable non-volatile photomemory effect in MoS2 transistors, 2D Mater. 6 (2019) 25036.
[12] S. Abbas, M. Kumar, D.-K. Ban, J.-H. Yun, J. Kim, Transparent and flexible in 2 O 3 thin film for multilevel nonvolatile photomemory programmed by light, ACS Appl. Electron. Mater. 1 (2019) 437–443, https://doi.org/10.1021/acsaelm.8b00139.
[13] T. Dixit, A. Tripathi, K.L. Ganapathi, M.S.R. Rao, V. Singh, Long-Lasting Persistent Photoconductivity in Au/CuO Thin Films for Optical Memory, vol. 32, 2020, pp. 329–332.
[14] G.Y. Lee, B.S. Mun, H. Ju, Observation of giant persistent photoconductivity on vanadium dioxide thin film device, Appl. Mater. Today 22 (2021) 100894.
[15] P.A. Hind, P.S. Patil, N.B. Gummagol, B. V Rajendra, Investigation of structure, morphology, photoluminescence, linear and third-order nonlinear optical properties of Sn1−xLaxO2 thin films for optical limiting applications, J. Alloys Compd. 892 (2021) 162070, https://doi.org/10.1016/j.jallcom.2021.162070.
[16] M.N. Rumyantseva, A.M. Gaskov, N. Rosman, T. Pagnier, J.R. Morante, D. Piscine, S. Martin, Raman Surface Vibration Modes in Nanocrystalline SnO 2 : Correlation with Gas Sensor Performances, 2005, pp. 893–901.
[17] V. Bonu, A. Das, A.K. Sivadasan, A.K. Tyagi, S. Dhara, Invoking Forbidden Modes in SnO 2 Nanoparticles Using Tip Enhanced Raman Spectroscopy, 2015, pp. 1037–1040, https://doi.org/10.1002/jrs.4747.
[18] A. Romano-rodrı, The Complete Raman Spectrum of Nanometric SnO 2 Particles, vol. 90, 2001, pp. 1550–1557, https://doi.org/10.1063/1.1385573.
[19] R.K. Mishra, S.K. Pandey, P.P. Sahay, Influence of in doping on the structural , photo-luminescence and alcohol response characteristics of the SnO 2 nanoparticles, Mater. Res. Bull. 48 (2013) 4196–4205, https://doi.org/10.1016/j.materresbull.2013.06.071.
[20] V.K. Reshmy, K.G. Gopchandran, V.K. Vaidyan, Optical and Raman studies of nanocrystallinetinoxide thin films prepared by spray pyrolysis, J. Optoelectron. Adv. Mater. 21 (2019) 609–617.
[21] C.M. Cunyi Xie, L.I.D.E. Zhang, Characterization of Raman Spectra in Nano-SnO2 Solids, vol. 59, 1994, pp. 59–61.
[22] L. Abello, B. Bochu, A. Gaskov, S. Koudryavtseva, G. Lucazeau, M. Roumyantseva, Structural Characterization of Nanocrystalline SnO 2 by X-Ray and Raman Spectroscopy, vol. 85, 1998, pp. 78–85.
[23] A. Romano-rodriguez, J.R. Morante, U. Weimar, M. Schweizer-berberich, W. Gpel, Morphological Analysis of Nanocrystalline SnO2 for Gas Sensor Applications, vol. 31, 1996, pp. 1–8.
[24] Z. Li, Q. Yang, Y. Wu, Y. He, J. Chen, J. Wang, La 3+ doped SnO 2 nanofibers for rapid and selective H 2 sensor with long range linearity, Int. J. Hydrogen Energy 44 (2019) 8659–8668, https://doi.org/10.1016/j.ijhydene.2019.02.050.
[25] Z. Xu, S.H. Teo, L. Gao, Z. Guo, Y. Kamata, S. Hayase, T. Ma, La-doped SnO2 as ETL for efficient planar-structure hybrid perovskite solar cells, Org. Electron. 73 (2019) 62–68, https://doi.org/10.1016/j.orgel.2019.03.053.
[26] C. Shi, Y. Zhu, Q. Xu, X. Tao, C. Kong, A study of ordered La-doped SnO2 nanofibers in light of their length and gas sensitivity, Phys. E Low-Dimensional Syst. Nanostructures. (2020) 114294, https://doi.org/10.1016/j.physe.2020.114294.
[27] X. Wang, Y. Zhang, Y. Wang, T. Ma, T. Liang, Lanthanum concentration dependence of electrical properties in tin oxide thin films, J. Mater. Sci. Mater. Electron. 24 (2013) 889–895.
[28] Y.N. Colmenares, S.H. Messaddeq, Y. Messaddeq, Studying the kinetics of microstructure formation through dewetting of As-Se thin films, Phys. Rev. Mater. (2021) 015605, https://doi.org/10.1103/PhysRevMaterials.5.015605, 1–10.
[29] Y. Liao, Y.J. Kim, J. Lai, J. Seo, M. Kim, Antireflective GaN nanoridge texturing by metal-assisted chemical etching via a thermally dewetted Pt catalyst network for highly responsive ultraviolet photodiodes. https://doi.org/10.1021/acsami.2c22929, 2023.
[30] J. Jeong, S.P. Choi, C.I. Chang, D.C. Shin, J.S. Park, B.T. Lee, Y.J. Park, H.J. Song, Photoluminescence properties of SnO2 thin films grown by thermal CVD, Solid State Commun. 127 (2003) 595–597, https://doi.org/10.1016/S0038-1098(03)00614-8.
[31] S. Sarmah, A. Kumar, Optical Properties of of SnO2 Nanoparticles, vol. 84, 2010, pp. 1211–1221.
[32] L. Dua, P.K. Biswas, Synthesis and photoluminescence property of nanostructured sol-gel antimony tin oxide film on silica glass, Chem. Phys. Lett. 572 (2013) 66–72, https://doi.org/10.1016/j.cplett.2013.04.015.
[33] C.G. Fonstad, R.H. Rediker, Electrical properties of high-quality stannic oxide crystals, J. Appl. Phys. 42 (1971) 2911–2918.

[34] S. Samson, C.G. Fonstad, Defect structure and electronic donor levels in stannic oxide crystals, J. Appl. Phys. 44 (1973) 4618–4621.
[35] J.D. Prades, J. Arbiol, A. Cirera, J.R. Morante, M. Avella, L. Zanotti, E. Comini, G. Faglia, G. Sberveglieri, Defect study of SnO2 nanostructures by cathodoluminescence analysis: application to nanowires, Sensors Actuators B Chem. 126 (2007) 6–12.
[36] M. Epifani, J.D. Prades, E. Comini, E. Pellicer, M. Avella, P. Siciliano, G. Faglia, A. Cirera, R. Scotti, F. Morazzoni, others, the role of surface oxygen vacancies in the NO2 sensing properties of SnO2 nanocrystals, J. Phys. Chem. C 112 (2008) 19540–19546.
[37] G. Zhang, S. Zhang, L. Yang, Z. Zou, D. Zeng, C. Xie, La2O3-sensitized SnO2 nanocrystalline porous film gas sensors and sensing mechanism toward formaldehyde, Sensors Actuators B Chem. 188 (2013) 137–146.
[38] M. Boomashri, P. Perumal, S. Vinoth, M. Shkir, S. AlFaify, Enhancement in room temperature ammonia sensing performance of the La substituted SnO2 (La: SnO2) thin films developed using spray pyrolysis technique, Phys. Scr. 97 (2022) 55808.
[39] C. Glynn, C.O. Dwyer, Solution processable metal oxide thin film deposition and material growth for electronic and photonic devices. https://doi.org/10.1002/admi.201600610, 2017.
[40] D. Gentili, G. Foschi, F. Valle, M. Cavallini, F. Biscarini, Applications of dewetting in micro and nanotechnology, Chem. Soc. Rev. 41 (2012) 4430–4443, https://doi.org/10.1039/c2cs35040h.
[41] M.N. Rumyantseva, O. V Safonova, M.N. Boulova, L.I. Ryabova, A.M. Gas' kov, Dopants in nanocrystalline tin dioxide, Russ. Chem. Bull. 52 (2003) 1217–1238.
[42] S.R. Dhage, V. Ravi, S.K. Date, Influence of lanthanum on the nonlinear I-V characteristics of SnO2: Co, Nb, Mater. Lett. 57 (2002) 727–729, https://doi.org/10.1016/S0167-577X(02)00861-3.
[43] H. Chen, L. Hu, X. Fang, L. Wu, General fabrication of monolayer SnO 2 nanonets for high-performance ultraviolet photodetectors, Adv. Funct. Mater. 22 (2012) 1229–1235, https://doi.org/10.1002/adfm.201102506.
[44] R. Ghosh, B. Mallik, D. Basak, Dependence of Photoconductivity on the Crystallite Orientations and Porosity of Polycrystalline ZnO Films, vol. 1284, 2005, pp. 1281–1284, https://doi.org/10.1007/s00339-004-3035-x.
[45] K. Selma, B. Salima, B. Seddik, R. Djamil, H. Lazhar, Investigation of UV photosensor properties of Al-doped SnO 2 thin films deposited by sol-gel dip-coating method. https://doi.org/10.1088/1674-4926/44/3/032801, 2023.
[46] K.M. Sandeep, S. Bhat, S.M. Dharmaprakash, P.S. Patil, K. Byrappa, Defect assisted saturable absorption characteristics in Al and Li doped ZnO thin films, J. Appl. Phys. 120 (2016), https://doi.org/10.1063/1.4963118.
[47] N. Prakash, K. Anand, A. Barvat, P. Pal, D.K. Singh, M. Jewariya, S. Ragam, S. Adhikari, K.K. Maurya, S.P. Khanna, The impact of RF-plasma power in carrier relaxation dynamics of unintentional doped GaN epitaxial layers grown by MBE, Opt. Mater. 54 (2016) 26–31.
[48] C. Zhang, G. Liu, X. Geng, K. Wu, M. Debliquy, Metal Oxide Semiconductors with Highly Concentrated Oxygen Vacancies for Gas Sensing Materials: A Review, Elsevier B.V., 2020, https://doi.org/10.1016/j.sna.2020.112026.
[49] Y. Huang, Y. Yu, Y. Yu, B. Zhang, Oxygen Vacancy Engineering in Photocatalysis, 2020, p. 2000037, https://doi.org/10.1002/solr.202000037, 1–14.
[50] I. Gupta, S. Singh, S. Bhagwan, D. Singh, Rare earth (RE) doped phosphors and their emerging applications: a review, Ceram. Int. 47 (2021) 19282–19303, https://doi.org/10.1016/j.ceramint.2021.03.308.
[51] F.R. Messias, L.V.A. Scalvi, M.S. Li, Photodesorption and Electron Trapping in N-type SnO 2 Thin Films Grown by dip-coating technique, 2006, pp. 37–41, https://doi.org/10.1080/10420159808220291.
[52] P. Dorenbos, Lanthanide charge transfer energies and related luminescence, charge carrier trapping, and redox phenomena, J. Alloys Compd. 488 (2009) 568–573, https://doi.org/10.1016/j.jallcom.2008.09.059.
[53] Q.L. Li, X.H. Zhang, T. Lin, K.H. Gao, Electrical transport properties of polycrystalline SnO2 thin films, J. Alloys Compd. 764 (2018) 295–299, https://doi.org/10.1016/j.jallcom.2018.06.090.
[54] M.S. Moreno, J.J. Kas, C. Ma, F. Wang, J.J. Rehr, M. Malac, Probing electronic structure of stoichiometric and defective Sn O2, Phys. Rev. B 95 (2017), https://doi.org/10.1103/PhysRevB.95.245206.
[55] A.K. Pal, Grain-boundary scattering in semiconductor films, Bull. Mater. Sci. 17 (1994) 1251–1258, https://doi.org/10.1007/BF02747224.
[56] J. Chao, D. Zhang, S. Xing, Y. Chen, W. Shen, Controllable assembly of tin oxide thin films with efficient photoconductive activity, Mater. Lett. 229 (2018) 244–247, https://doi.org/10.1016/j.matlet.2018.07.027.
[57] M. Al-Hashem, S. Akbar, P. Morris, Role of oxygen vacancies in nanostructured metal-oxide gas sensors: a review, Sensors Actuators, B Chem. 301 (2019) 126845, https://doi.org/10.1016/j.snb.2019.126845.
[58] D.F. Cox, T.B. Fryberger, S. Semancik, Oxygen vacancies and defect electronic states on the SnO2(110)-1×1 surface, Phys. Rev. B 38 (1988) 2072–2083, https://doi.org/10.1103/PhysRevB.38.2072.
[59] J. Dai, E. Frantzeskakis, F. Fortuna, P. Lömker, R. Yukawa, M. Thees, S. Sengupta, P. Le Fèvre, F. Bertran, J.E. Rault, K. Horiba, M. Müller, H. Kumigashira, A. F. Santander-Syro, Tunable two-dimensional electron system at the (110) surface of SnO2, Phys. Rev. B 101 (2020) 1–10, https://doi.org/10.1103/PhysRevB.101.085121.
[60] M. Batzill, K. Katsiev, U. Diebold, Surface Morphologies of SnO 2 (1 1 0), vol. 529, 2003, pp. 295–311, https://doi.org/10.1016/S0039-6028(03)00357-1.
[61] E.A. Floriano, L.V.A. Scalvi, J.R. Sambrano, A. De Andrade, Applied Surface Science Decay of photo-induced conductivity in Sb-doped SnO 2 thin films , using monochromatic light of about bandgap energy, Appl. Surf. Sci. 267 (2013) 164–168, https://doi.org/10.1016/j.apsusc.2012.09.003.
[62] T. Ganesh, S. Rajesh, F.P. Xavier, Photoconducting and photoresponse studies on multilayered thin films of aluminium doped zinc oxide, Indian J. Sci. Technol. 5 (2012) 2360–2363, https://doi.org/10.17485/ijst/2012/v5i3.9.
[63] J. Yao, Z. Zheng, G. Yang, An innovative postdeposition annealing approach producing centimeter-scale In2O3/in2 (TeO3) 3 bulk heterojunction thin film for room-temperature persistent photoconductivity, Adv. Opt. Mater. 5 (2017) 1600908.